Automatic Tuberculosis Detection using Binary Pattern of Phase Congruency

Type: Full/Regular Research Paper
Track: CSCI-RTHI

Afonso Ueslei da Fonseca*, Juliana Paula Felix*, Gabriel da Silva Vieira*†, Deborah Fernandes* and Fabrizzio Soares*
*Universidade Federal de Goiás, Goiânia – GO, Brazil.
†Instituto Federal Goiano, Campus Ceres, Ceres – GO, Brazil.
{afonsoueslei, julianafelix, deborah.fernandes, fabrizzio}ufg.br, {gabriel.vieira}@ifgoiano.edu.br,

***Abstract*—Computational solutions to assist the automatic analysis of radiographic images are already a reality. Commercial solutions for the diagnosis of tuberculosis have shown exceptional results similar to those of radiologists. However, these solutions are still far from regions of greater vulnerability, given their high costs. Researchers have shown a growing interest in developing increasingly efficient and effective solutions that require the least resources. Thus, in this work, we explore the use of chest X-ray and Phase Congruence Binary Pattern features to build a minimalist, low computational cost, and high-efficiency Feed-Forward Neural Network model to aid the diagnosis of tuberculosis. Our results showed high performance compared to related research, placing our solution as a viable alternative.**

***Index Terms*—artificial neural network, tuberculosis detection, chest X-ray, binary pattern of phase congruency.**

I. Introduction

Although Tuberculosis (TB) is preventable, treatable, and curable, it still represents a serious public health problem worldwide, mainly affecting the most vulnerable populations. The high costs of the entire health chain do with these populations not even seeking a diagnosis, implying directly not only the lack of treatment but also the underreporting of the disease [1]. The World Health Organization (WHO) shows that, only in 2020, 10 million people were infected worldwide and 1.5 million died by TB [2]. Therefore, affordable and scalable solutions, low-cost, of rapid response, and easy implementation are essential in fighting tuberculosis to aid in correctly screening, triaging, and diagnosing patients.

A recent WHO report pointed to a risk in global progress in fighting TB, which after decades of progress, showed, for the first time since 2005, an increase in cases and deaths in 2020. The reduction in diagnosis and treatment was possibly caused by reflections of the SARS-CoV-19 pandemic [3]. Although the WHO has presented the eradication of TB by 2030 as one of its goals [4], this action must be supported by public health services, for which access remains a challenge, especially in developing countries.

In recent decades, Artificial Intelligence (AI) has proven to be a useful tool to assist medical professionals in interpreting, screening, or even diagnosing diseases. In particular, the diagnosis of TB on chest radiographs (CXR) using AI techniques has emerged as an area of great research interest [5]. Thus, the availability of new computational tools that help diagnose TB and, in particular, smart, speedy, low-cost, and highly effective solutions, consists of an area of interest for study. Furthermore, new solutions may prove to be an alternative for developing countries, which not only tend to have a higher rate of co-infection, but also suffer from a shortage of radiologists [6], making early and accurate diagnosis of TB more difficult.

Several computational techniques and artificial intelligence methods have been presented, from classical machine learning to deep learning (DL) [7]–[11]. In addition to the machine learning method, such approaches vary in the way they extract features from CXR images and select the final set, which can occur manually or automatically [12]–[14]. For example, among the feature extraction methods previously used, are those extracted through intensity histograms, gradient magnitude, oriented gradient and oriented gradient pyramid, shape, texture, color and edge descriptors, Local Binary Pattern (LBP), and Speeded-up Robust Features (SURF).

Among the machine learning methods, the most used are Support Vector Machines (SVM), Multilayer Perceptron (MLP), and Linear Logistic Regression (LLR). In addition, Feed-Forward Neural Networks (FFNN), the first and simplest categories of artificial neural networks (ANN) developed [15], were also used in research related to TB [16]–[18]. One of the advantages of FFNNs is the balance between the necessary resources (less than DL models) and its performance or predictive capacity, which is independent of data probability distribution information.

In this sense, we aim to contribute with this area presenting a low-cost and high-efficiency computational solution specially developed for regions, environments and equipment with few resources, that assist in diagnosing tuberculosis cases. Our proposal is based on constructing an FFNN and the innovative extraction of features of the Binary Phase Congruence Pattern (BPPC) from CXR images to build a model for diagnosing TB cases among non-TB cases (healthy patients and sick non-TB).

There are few literature reports of phase congruence (PC) [19] methods for analyzing TB cases on CXR. Rijal *et al.* [20] extracted first-order statistical features calculated from six distinct zones of CXR-derived PC images to measure the

Corresponding Author: Afonso Ueslei da Fonseca – afonsoueslei@ufg.br

979-8-3503-2028-2/22/$31.00 ©2022 IEEE
DOI 10.1109/CSCI58124.2022.00053

transition between healthy and TB-infected lung tissue pixels. Ebrahimian et *al.* [21] combined PC and linear discriminant classifiers in an algorithm to differentiate the manifestations of TB and pneumonia on chest radiography. BPPC, an LBP adaptation using PC, was first used for facial recognition [22] and later in other applications [23], [24], being only one of those applied to CXR images [25].

Thus, our proposal is the first work, as far as we know, to use the extraction of BPPC features from CXR images and apply it to the analysis of Tuberculosis cases. The results point to a quick, inexpensive solution with high specificity that requires low consumption of computational resources, proving to be an alternative to aid in diagnosing TB.

II. Materials and Methods

In this section, the main steps of the proposed method are described, in which the BPPC features are extracted from the CXR images, and the FFNN model is built and trained for TB and Non-TB classification. In addition, brief descriptions of the materials, algorithms, and techniques used in the proposal are also provided, followed by references that provide more information about them.

A. Database Description

TBX11K dataset established by Liu et al. [8] in cooperation with several hospitals originally consists of 11200 unique CXRs, with a resolution size of 512×512 pixels, distributed across 5000 healthy cases, 5000 sick cases without TB, and 1200 cases with TB manifestations. Among the 1200 TB manifestations cases are active TB infections, latent TB, and both (active and latent TB). There are also among these 10 cases with uncertain TB whose types of TB infection cannot be recognized in current medical conditions. The TBX11K also comprises CXR images from the DA [26] , DB [26], Montgomery (MC) [27] and Shenzhen (SHZ) [27] sets.

All CXR images in TBX11K dataset were labeled following the gold standard and then divided into training, validation, and testing subsets. The labels associated with each case were provided for the training and validation subsets, while for the testing subset, they are not available. Thus, considering the unavailability of labels for the test subset's CXR images, we only use the 8976 CXR images with available labels, which are distributed according to Table I.

TABLE I: Brief description of the TBX11K used in this study.

	Class	Samples	Subtotal
Non-TB	Healthy	3800 (42.33%)	7600 (84.67%)
	Sick & Non-TB	3800 (42.33%)	
TB	Active TB	630 (7.02%)	1376 (15.33%)
	Latent TB	140 (1.56%)	
	Both (Active & Latent)	30 (0.33%)	
	DA & DB [26]	176 (1.96%)	
	MC & SHZ [27]	400 (4.45%)	
	TOTAL		**8976 (100%)**

B. Binary Pattern of Phase Congruency (BPPC)

Binary Pattern of Phase Congruency (BPPC) is an adaptation to Local Binary Patterns (LBP), where the intensity value needed to calculate the traditional LBP is replaced by the Phase Congruence (PC) [19] value in the corresponding *pixel*. PC models are, in turn, essential pattern descriptors, as they provide a measure independent of the overall signal magnitude, making it invariant to image illumination and contrast variations. Thus, as the PC image describes different feature categories, the LBP code is also designed to describe different categories.

The first step in BPPC is finding the image's PC in different orientations. Then, taking four directions and dividing the frequency plane uniformly, the resulting input image features are obtained by concatenating each BPPC image's histogram in one direction. For each, the same number adopted in [28] of 177 bins was used so that the final vector has 708 features. The BPPC feature extraction process is shown in Figure 1 with an input CXR image, its PC images, followed by the corresponding BPPC images, and finally, the BPPC histogram representing the extracted features.

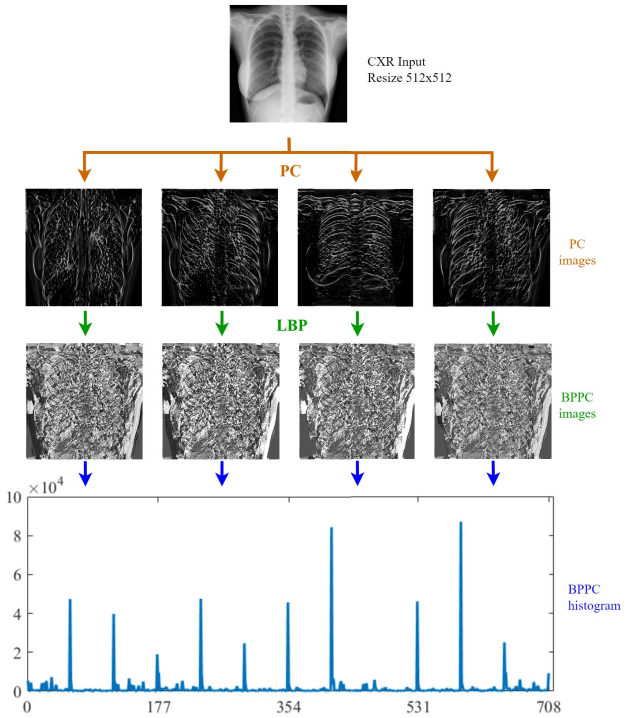

Fig. 1: The BPPC feature extraction process to an input CXR.

C. Feed-Forward Networks

Feed-Forward neural networks (FFN) were the first and simplest categories of artificial neural networks developed [15]. In these networks, connections between nodes do not form a loop, so information only moves in one direction – forwards – from input layer nodes, through hidden layer nodes, to data layer nodes output [29].

In this study, we have chosen these networks for their great predictive capacity, independent of data probability distribution information. This is important in clinical research, as its events may have a non-specific distribution. Furthermore, these networks have been successfully applied in a wide range of medical applications, including Alzheimer's disease [30], chronic kidney disease [31], lung cancer detection [32] and prediction of outbreaks of COVID-19 [33]. The parallel structure and the ability to improve performance through experience explain the efficiency of these networks.

Thus, in this study, we built a specific Feed-Forward Neural Network Model configured with a single hidden layer of three neurons fed with features obtained in the first step by BPPC. Figure 2 shows the structure of our model, which is designed to classify CXR images between TB and non-TB cases. This reduced structure guarantees fast training, low consumption of computational resources, and high performance for the network. Furthermore, we use the Levenberg-Marquardt [34] backpropagation training function, which updates the weights (w) and bias (b); Softmax transfer function; Learning rate 0.001; Active function *Tansig*; A maximum number of epochs equal to 20 and a maximum number of validation failures equal to 5 to avoid overfitting.

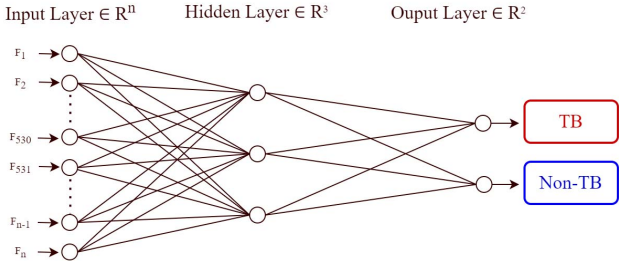

Fig. 2: FFN with n input nodes, 1 hidden layer with 3 neurons, and the output layer to the binary classification scheme, TB versus Non-TB cases.

D. Evaluation

This study used cross-validation (CV) with ten folds (stratified by incidence class), to measure the model's generalizability. This technique divides samples from a dataset into mutually exclusive subsets used in the training and testing rounds. The CV thus measures how the results of a statistical analysis of the model generalize to an independent dataset. In problems where the modeling objective is classification, CV is widely used [35].

E. Evaluation Measures

We used the following evaluation measures: *Accuracy (ACC)* which represents the hit rate among the total number of cases examined; *Sensitivity or True Positive Rate (TPR)* which represents the rate of individuals belonging to the positive class (TB cases) who were correctly identified as TB, and *Specificity or True Negative Rate (TNR)* which measures the percentage of people belonging to the negative class (Healthy or Sick Non-TB cases) that were correctly identified. Therefore, finalized $10-CV$ process in test cases, the results of their measurements are reported for each fold, followed by the absolute mean and standard deviation. In addition, the Receiver Operating Characteristic (ROC) curves of the model, a Sankey diagram [36] resulting, and the value of the Diagnostic Odds Ratio (DOR) [37] are calculated.

F. Environment Setting

The experiments were conducted on a desktop Core$^{(TM)}$ CPU5-62Ghz, 2.3Ghz, 2GB of RAM, installed with Windows 10 64-bit and MATLAB© R2014a with the packages *Deep Learning Toolbox* and *Signal Processing Toolbox*. The equipment did not have GPU-accelerated graphics processing.

III. Results and Discussion

This section presents our model's results and a brief discussion. In addition, comparisons with the literature are also drawn to position the results achieved in this work.

A. Performance of Model: Binary Classification

In this model, TBX11K samples are divided into two classes: TB and Non-TB, to detect TB cases among healthy individuals or those with a disease other than TB. We then evaluated the model's performance using only the features extracted from each CXR image.

All features were extracted directly from the 1376 images of the TB class and the 7600 images of the Non-TB class, according to the division seen in Table I. Thus, in Table II the matrix of confusion, ACC, TPR, and TNR are shown for each cross-validation process fold; at the end, the consolidated result is accompanied by the standard deviation. We can see from the results that the model has a high and consistent TNR with low variance between folds. Regarding the TPR, the lower value and the higher variance between skinfolds can be explained by the imbalance between classes, with a lower number of TB samples.

TABLE II: Model - Binary Classification

Fold	ACC	TPR	TNR	Confusion Matrix			
				TP	FP	TN	FN
1	95.09%	85.4%	96.8%	117	24	736	20
2	97.55%	94.9%	98.0%	131	15	745	7
3	99.78%	99.3%	99.9%	137	1	759	1
4	99.67%	99.3%	99.7%	137	2	758	1
5	99.67%	98.6%	99.9%	136	1	759	2
6	100.00%	100.0%	100.0%	138	0	760	0
7	99.00%	99.3%	98.9%	137	8	752	1
8	99.78%	100.0%	99.7%	137	2	758	0
9	99.33%	100.0%	99.2%	137	6	754	0
10	99.11%	98.5%	99.2%	135	6	754	2
Total	**98.90±1.51%**	**97.52±4.51%**	**99.14±1%**	**1342**	**65**	**7535**	**34**

TP: True positive (TB cases), **TN:** True negative (Non-TB cases), **FP:** False positive, **FN:** False negative.

Figure 3(a) shows the receiver operating characteristic (ROC) of the model, which explains its high performance by showing an ideal operating point pointing to an area under the ROC curve (AUC) of 0.99 , stable across different rank thresholds. At the same time, the Sankey diagram in Figure 3(b)

presents a new way of looking at model performance through the flows of its instances from input to output. Thus, in this diagram, the flows between input and output instances with crossed classes represent the misclassifications of the model (such as FN and FP of the confusion matrix), while the direct flows between classes are the hits. The more insignificant or non-existent the fractions of cross-flows (incorrect) and the greater the fractions of direct flows (correct), the better the model. Thus, the thin crossed lines shown in the diagram represent a model with low errors and high accuracy. Finally, this model scores with a remarkable DOR value equal to $4,575.55$

Regarding class imbalance, more samples from the non-TB class reflect the actual clinical practice scenario. So while we have not addressed the issue of class balancing in the scope of this work, it is not neglected, and our future works have addressed this. For now, we bring the result of the Balanced Accuracy ($bACC$) [38] calculation with a value of 98.33%, showing that our method achieves high performance even considering this measure.

B. Auspicious Settings

As mentioned before, our model was thought and designed for use in regions, environments, and equipment with few resources (physical, financial, computational). Therefore, model characteristics such as time (building, training, and testing) and size (storage space, processing memory, etc.) are essential for its adoption as a solution. So while models based on deep neural networks are unquestionable in many tasks and the first choice of many solutions, they fail in some respects because they are built with thousands of parameters, require high processing power and time, and sometimes are difficult to interpret. Also, DL models often require parallel processing using expensive equipment. Thus, our proposal based on shallow artificial neural networks has higher parameter efficiency, only 872 input features, and a single hidden layer with only three neurons; therefore, fewer degrees of freedom and less prone to overfitting. Also, using standard desktop equipment with no acceleration or graphics memory, extracting BPPC features takes an average of $0.57s$ per CXR image. For model building and training, the memory required is less than $200Kb$ with an average of $0.15s$ to process each image. Once the model is trained, it takes just $7ms$ to infer a new input.

C. Comparison of Results with Related Literature

In Table III we bring a brief comparison of the results obtained with other recent works in the literature that make the detection of tuberculosis. Given the limited number of studies using the TBX11K database, we included in this comparison studies that used other databases known in the literature.

Although the works use different methodologies, datasets, and data-splitting schemes, the comparison still provides a state-of-the-art view of tuberculosis detection and supports the evaluation of our proposal.

Our proposal is not yet a commercial solution; however, it still stands out compared to those already available. According

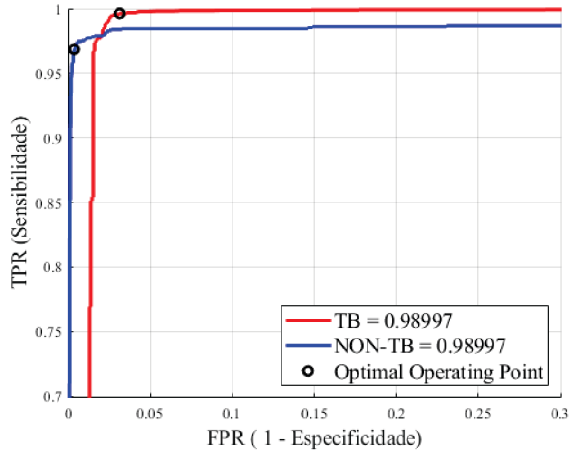

(a) ROC curves

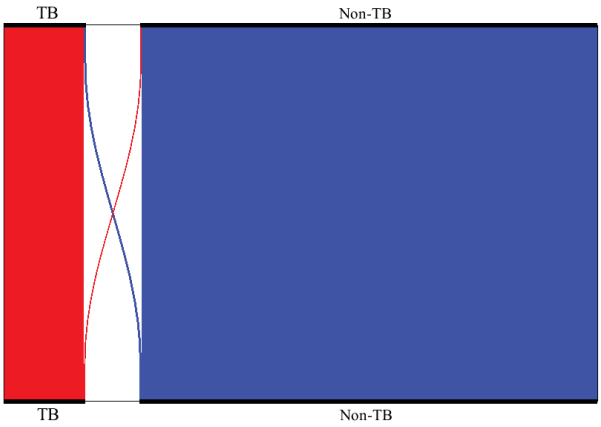

(b) Sankey diagram

Fig. 3: ROC curves in zoom and Sankey Diagram resulting of our overall binary classification model.

to an independent evaluation by Codlin *et al.* [39] of 12 commercial artificial intelligence solutions for tuberculosis screening, the best AUC values achieved were between 0.70-0.86 for a 95% confidence interval (CI) when combining the sensitivity of an Expert Reader, the TPR and TNR were between 90.4-98.3% and 42-52%, respectively. Although not submitted to the same evaluative rigor as Codlin, the results of our model showed more expressive values, reaching a DOR value of 4,575.55.

IV. Conclusions

This work presented a smart, speedy, low-cost, high-efficiency computational solution to assist to diagnose tuberculosis cases. Based on an experimental evaluation in an extensive public TB database called TBX11K, the proposed method is assertive in diagnosing TB cases, considering whole CXR images as input. As a novelty, our method is the first to use CXR BPPC feature extraction to diagnose TB and requires

TABLE III: Comparison of tuberculosis detection with some related works

Year	Study	Methodology	Dataset	Partition (%) train/val/test	Test results (%) ACC±σ	TPR	TNR	AUC
2018	Vajda *et al.* [12]	① FE(SetA,B,C), FS weary, MLP	MC	10-CV	84.7±11.16	-	-	91.0
			SH		97.0±1.71	-	-	99.0
2019	Singh & Hamde [40]	① FE(SetA,B), SVM	MC	≈64/36	96.0	91.0	100	98.0
			SH	≈17/7	97.8	95.0	100	96.0
2019	Pasa *et al.* [41]	② Custom CNN model	MC	5-CV	79.0	-	-	81.1
			SH		84.4	-	-	90.0
2019	Gozes & Greenspan [42]	② ChexNet	MC	$\approx 77/11^{SH}$/MC	-	-	-	95.2
		② MetaChexNet (DFE+Metadata)	SH	≈77/11/11	-	-	-	96.5
		② ChexNet	MCSH	≈77/11/11+MC	-	-	-	94.4
2020	Sahlol *et al.* [43]	② DFE(MobileNet), Metaheuristic	SH	80/20	90.20	91.94	90.14	-
2021	Oltu *et al.* [44]	② DFE(MobileNet), SVM	SH	5-CV	96.6	-	-	99.0
2021	Karaca *et al.* [14]	② DFE from 5 DCNNs, SVM	MC	5-CV	98.9	-	-	100
2021	Rajaraman *et al.* [10]	③ VGG-16 Fine-tuned	SH,BE,IND	80/20	92.3	96.9	85.6	95.3
2022	Fonseca *et al.* [13]	① FE(LBP), FS(MBO), KNN	MC	10-CV	83.3±7.16	65.50	96.25	82.9
			SH		90.3±3.06	85.42	95.4	92.4
			MCSH		87.0±3.29	80.0	93.8	88.9
2022	Nafisah & Muhammad [11]	① EfficientNetB3, DA	MC	5-CV	89.9	89.3	90.7	-
		① InceptionRenNetV2, DA	SH		93.7	93.6	93.8	-
		① EfficientNetB3, DA	MCSH		98.7	98.3	99.0	-
2020	Liu *et al.* [8]	② Faster R-CNN (ResNet w/FPN)	TBX11K	≈59/16/25	89.70	91.20	89.90	93.60
2022	Ngoc *et al.* [9]	③ EfficientNet-B5-FPA(KD)	TBX11K	≈94/2/4	96.8	88.5	97.9	96.7
2022	**Our proposed**	② FE(BPPC), FFNN	TBX11K	10-CV	98.90±1.51	97.52	99.14	99.0

FE: Feature extraction process, **DFE:** Deep feature extraction process, **FS:** Feature selection process, **LLR:** Linear Logistic Regression, **DA** Data augmentation. **SetA:**{IH, GM, SD, LD, HOG, LBP}, **SetB:**{Tamura Texture Descriptor, CEDD and FCTH, Hu Moments, CLD and EHD, Primitive Path, Edge Frequency, Autocorrelation and Shape Features}, **SetC:**{ Shape measurements as size, orientation, eccentricity, extent and centroid}, **MC:** Montgomery and **SH:** Shenzhen dataset [27], **MCSH:** MC and SH, **IND:** India dataset [26], NIADID [45] and RSNA [46] datasets. *In partition:* train/val/test or train/test percents, **LOOCV:** Leave-One-Out cross validation, **n-CV** n-folds cross validation. ①: Lung mask segmentation, ②: None segmentation and ③: Box crop segmentation.

no image pre-processing steps. The low standard deviation of the evaluation measures in the folds of the cross-validation process shown in the model proves the ability and stability of the proposal. In addition, our method built on FFNN models and BPPC resources, requires few computational requirements, memory, time, and energy, presenting results equivalent to those in the literature.

The results of our proposal for different assessment measures behave stably and show significant values of ACC, TPR, TNR, AUC, DOR, and bACC. For the same TBX11K dataset, our proposal outperforms the previous work with a significant margin and gets an AUC value of 0.99, while a sensitivity of 97.52% and a remarkable DOR value of $4,575.55$. Furthermore, using a Sankey diagram, a new visual way of evaluating through input and output flows, our model showed low cross-flows with fine lines of misclassification and high accuracy. Finally, the built model demonstrated that BPPC resources are valuable and effective in discriminating TB cases in CXR images, representing a valid alternative in constructing computational solutions by artificial intelligence for TB diagnosis.

ACKNOWLEDGMENT

This study was financed in part by the Coordenação de Aperfeiçoamento de Pessoal de Nível Superior – Brasil (CAPES) – Finance Code 001. The authors also thank Instituto Federal Goiano, câmpus Urutaí, for the financial support.

REFERENCES

[1] W. H. Organization *et al.*, "World health statistics 2022: monitoring health for the sdgs, sustainable development goals," 2022.
[2] WHO, "Global tuberculosis report 2021," p. 1, 2021.
[3] UN, "The sustainable development goals report 2022," https://unstats.un.org/sdgs/report/2022, 2022, accessed: 2022-07-17.
[4] N. CEPAL, "The 2030 agenda and the sustainable development goals: An opportunity for latin america and the caribbean," 2018.
[5] L. M. Pinto, M. Pai, K. Dheda, K. Schwartzman, D. Menzies, and K. R. Steingart, "Scoring systems using chest radiographic features for the diagnosis of pulmonary tuberculosis in adults: a systematic review," *European Respiratory Journal*, vol. 42, no. 2, pp. 480–494, 2013.
[6] S. Kulkarni and S. Jha, "Artificial intelligence, radiology, and tuberculosis: a review," *Academic radiology*, vol. 27, no. 1, pp. 71–75, 2020.
[7] P. Lakhani and B. Sundaram, "Deep learning at chest radiography: automated classification of pulmonary tuberculosis by using convolutional neural networks," *Radiology*, vol. 284, no. 2, pp. 574–582, 2017.
[8] Y. Liu, Y.-H. Wu, Y. Ban, H. Wang, and M.-M. Cheng, "Rethinking computer-aided tuberculosis diagnosis," in *2020 IEEE/CVF Conference on Computer Vision and Pattern Recognition (CVPR)*, 2020, pp. 2643–2652.

[9] H. Nguyen Ngoc, V. Hoang, T. H. Bui, S. Q. H. Truong, T. H. Minh, D. Nguyen Van, T. Nguyen Thi Minh, and C. Cung Van, "An efficient approach for tuberculosis diagnosis on chest x-ray," in *2022 IEEE 19th International Symposium on Biomedical Imaging (ISBI)*, 2022, pp. 1–5.

[10] S. Rajaraman, L. R. Folio, J. Dimperio, P. O. Alderson, and S. K. Antani, "Improved semantic segmentation of tuberculosis—Consistent findings in chest x-rays using augmented training of modality-specific U-Net models with weak localizations," *Diagnostics*, vol. 11, no. 4, p. 616, 2021.

[11] S. I. Nafisah and G. Muhammad, "Tuberculosis detection in chest radiograph using convolutional neural network architecture and explainable artificial intelligence," *Neural Computing and Applications*, pp. 1–21, 2022.

[12] S. Vajda, A. Karargyris, S. Jaeger, K. Santosh, S. Candemir, Z. Xue, S. Antani, and G. Thoma, "Feature selection for automatic tuberculosis screening in frontal chest radiographs," *Journal of medical systems*, vol. 42, no. 8, pp. 1–11, 2018.

[13] A. U. Fonseca, B. M. Rocha, E. A. Nogueira, G. S. Vieira, D. S. A. Fernandes, J. C. Lima, J. C. Ferreira, and F. Soares, "Tuberculosis Detection in Chest Radiography - A Combined Approach of Local Binary Pattern Features and Monarch Butterfly Optimization Algorithm," in *2022 IEEE 46th Annual Computers, Software, and Applications Conference (COMPSAC)*. IEEE, 2022, pp. 1408–1413.

[14] B. K. Karaca, S. Güney, B. Dengiz, and M. Ağıldere, "Comparative study for tuberculosis detection by using deep learning," in *2021 44th International Conference on Telecommunications and Signal Processing (TSP)*, 2021, pp. 88–91.

[15] J. Schmidhuber, "Deep learning in neural networks: An overview," *Neural networks*, vol. 61, pp. 85–117, 2015.

[16] O. Er, F. Temurtas, and A. Ç. Tanrıkulu, "Tuberculosis disease diagnosis using artificial neural networks," *Journal of medical systems*, vol. 34, no. 3, pp. 299–302, 2010.

[17] A. Fojnica, A. Osmanović, and A. Badnjević, "Dynamical model of tuberculosis-multiple strain prediction based on artificial neural network," in *2016 5th Mediterranean Conference on Embedded Computing (MECO)*, 2016, pp. 290–293.

[18] S. Khobragade, A. Tiwari, C. Patil, and V. Narke, "Automatic detection of major lung diseases using chest radiographs and classification by feed-forward artificial neural network," in *2016 IEEE 1st International Conference on Power Electronics, Intelligent Control and Energy Systems (ICPEICES)*, 2016, pp. 1–5.

[19] P. Kovesi *et al.*, "Image features from phase congruency," *Videre: Journal of computer vision research*, vol. 1, no. 3, pp. 1–26, 1999.

[20] O. Mohd Rijal, H. Ebrahimian, and N. M. Noor, "Determining features for discriminating ptb and normal lungs using phase congruency model," in *Proceedings of 2012 IEEE-EMBS International Conference on Biomedical and Health Informatics*, 2012, pp. 341–344.

[21] H. Ebrahimian, O. M. Rijal, N. M. Noor, A. Yunus, and A. A. Mahyuddin, "Phase congruency parameter estimation and discrimination ability in detecting lung disease chest radiograph," in *2014 IEEE Conference on Biomedical Engineering and Sciences (IECBES)*, 2014, pp. 729–734.

[22] S. Shojaeilangari, W.-Y. Yau, J. Li, and E.-K. Teoh, "Feature extraction through binary pattern of phase congruency for facial expression recognition," in *2012 12th International Conference on Control Automation Robotics & Vision (ICARCV)*, 2012, pp. 166–170.

[23] D. Dall'Alba and P. Fiorini, "Bipco: ultrasound feature points based on phase congruency detector and binary pattern descriptor," *International journal of computer assisted radiology and surgery*, vol. 10, no. 6, pp. 843–854, 2015.

[24] L. Cai, X. Wang, Y. Wang, Y. Guo, J. Yu, and Y. Wang, "Robust phase-based texture descriptor for classification of breast ultrasound images," *Biomedical engineering online*, vol. 14, no. 1, pp. 1–21, 2015.

[25] A. U. Fonseca, J. P. Felix, G. S. Vieira, D. S. A. Fernandes, and F. Soares, "Artificial neural networks and bppc features for detecting covid-19 and severity level," in *2022 IEEE International Conference on Systems, Man, and Cybernetics (SMC)*, 2020, pp. 4346–4351.

[26] A. Chauhan, D. Chauhan, and C. Rout, "Role of gist and phog features in computer-aided diagnosis of tuberculosis without segmentation," *PloS one*, vol. 9, no. 11, p. e112980, 2014.

[27] S. Jaeger, S. Candemir, S. Antani, Y.-X. J. Wáng, P.-X. Lu, and G. Thoma, "Two public chest x-ray datasets for computer-aided screening of pulmonary diseases," *Quantitative imaging in medicine and surgery*, vol. 4, no. 6, p. 475, 2014.

[28] C. Turan and K.-M. Lam, "Histogram-based local descriptors for facial expression recognition (FER): A comprehensive study," *Journal of visual communication and image representation*, vol. 55, pp. 331–341, 2018.

[29] A. Zell, *Simulation neuronaler netze*. Addison-Wesley Bonn, 1994, vol. 1.

[30] S. Wang, Y. Zhang, Z. Dong, S. Du, G. Ji, J. Yan, J. Yang, Q. Wang, C. Feng, and P. Phillips, "Feed-forward neural network optimized by hybridization of pso and abc for abnormal brain detection," *International Journal of Imaging Systems and Technology*, vol. 25, no. 2, pp. 153–164, 2015.

[31] N. A. Almansour, H. F. Syed, N. R. Khayat, R. K. Altheeb, R. E. Juri, J. Alhiyafi, S. Alrashed, and S. O. Olatunji, "Neural network and support vector machine for the prediction of chronic kidney disease: A comparative study," *Computers in biology and medicine*, vol. 109, pp. 101–111, 2019.

[32] R. Arulmurugan and H. Anandakumar, "Early detection of lung cancer using wavelet feature descriptor and feed forward back propagation neural networks classifier," in *Computational vision and bio inspired computing*. Springer, 2018, pp. 103–110.

[33] A. J. Aljaaf, T. M. Mohsin, D. Al-Jumeily, and M. Alloghani, "A fusion of data science and feed-forward neural network-based modelling of covid-19 outbreak forecasting in IRAQ," *Journal of Biomedical Informatics*, vol. 118, p. 103766, 2021.

[34] S. Sapna, A. Tamilarasi, M. P. Kumar *et al.*, "Backpropagation learning algorithm based on levenberg marquardt algorithm," *Comp Sci Inform Technol (CS and IT)*, vol. 2, pp. 393–398, 2012.

[35] R. Kohavi *et al.*, "A study of cross-validation and bootstrap for accuracy estimation and model selection," in *Ijcai*, vol. 14.2. Montreal, Canada, 1995, pp. 1137–1145.

[36] T. Keiderling, "Der brockhaus," *Groβe Lexika und Wörterbücher Europas: Europäische Enzyzklopädien und Wörterbücher in historischen Porträts*, pp. 193–210, 2012.

[37] A. S. Glas, J. G. Lijmer, M. H. Prins, G. J. Bonsel, and P. M. Bossuyt, "The diagnostic odds ratio: a single indicator of test performance," *Journal of clinical epidemiology*, vol. 56, no. 11, pp. 1129–1135, 2003.

[38] J. P. Mower, "Prep-mt: predictive rna editor for plant mitochondrial genes," *BMC bioinformatics*, vol. 6, no. 1, pp. 1–15, 2005.

[39] A. J. Codlin, T. P. Dao, L. N. Q. Vo, R. J. Forse, V. Van Truong, H. M. Dang, L. H. Nguyen, H. B. Nguyen, N. V. Nguyen, K. Sidney-Annerstedt *et al.*, "Independent evaluation of 12 artificial intelligence solutions for the detection of tuberculosis," *Scientific Reports*, vol. 11, no. 1, pp. 1–11, 2021.

[40] N. Singh and S. Hamde, "Tuberculosis detection using shape and texture features of chest x-rays," in *Innovations in Electronics and Communication Engineering*. Springer, 2019, pp. 43–50.

[41] F. Pasa, V. Golkov, F. Pfeiffer, D. Cremers, and D. Pfeiffer, "Efficient deep network architectures for fast chest x-ray tuberculosis screening and visualization," *Scientific reports*, vol. 9, no. 1, pp. 1–9, 2019.

[42] O. Gozes and H. Greenspan, "Deep feature learning from a hospital-scale chest x-ray dataset with application to TB detection on a small-scale dataset," in *2019 41st annual international conference of the ieee engineering in medicine and biology society (embc)*. IEEE, 2019, pp. 4076–4079.

[43] A. T. Sahlol, M. Abd Elaziz, A. Tariq Jamal, R. Damaševičius, and O. Farouk Hassan, "A novel method for detection of tuberculosis in chest radiographs using artificial ecosystem-based optimisation of deep neural network features," *Symmetry*, vol. 12, no. 7, p. 1146, 2020.

[44] B. Oltu, S. Güney, B. Dengiz, and M. Ağıldere, "Automated Tuberculosis Detection Using Pre-Trained CNN and SVM," in *2021 44th International Conference on Telecommunications and Signal Processing (TSP)*, 2021, pp. 92–95.

[45] A. Rosenthal, A. Gabrielian, E. Engle, D. E. Hurt, S. Alexandru, V. Crudu, E. Sergueev, V. Kirichenko, V. Lapitskii, E. Snezhko *et al.*, "The tb portals: an open-access, web-based platform for global drug-resistant-tuberculosis data sharing and analysis," *Journal of clinical microbiology*, vol. 55, no. 11, pp. 3267–3282, 2017.

[46] X. Wang, Y. Peng, L. Lu, Z. Lu, M. Bagheri, and R. M. Summers, "Chestx-ray8: Hospital-scale chest x-ray database and benchmarks on weakly-supervised classification and localization of common thorax diseases," in *Proceedings of the IEEE conference on computer vision and pattern recognition*, 2017, pp. 2097–2106.